Experimental Evidence of Plasmophores: Plasmon-Directed Polarized Emission from Gold Nanorod-Fluorophore Hybrid Nanostructures

ARTICLE *in* NANO LETTERS · JUNE 2011

Impact Factor: 13.59 · DOI: 10.1021/nl200535y · Source: PubMed

6 AUTHORS, INCLUDING:

Tian Ming
Massachusetts Institute of Technology
40 PUBLICATIONS **1,699** CITATIONS
SEE PROFILE

Lei Zhao
Nanjing University
95 PUBLICATIONS **860** CITATIONS
SEE PROFILE

NANO LETTERS

LETTER

pubs.acs.org/NanoLett

Experimental Evidence of Plasmophores: Plasmon-Directed Polarized Emission from Gold Nanorod−Fluorophore Hybrid Nanostructures

Tian Ming,[†] Lei Zhao,[†] Huanjun Chen,[†] Kat Choi Woo,[†] Jianfang Wang,[*,†] and Hai-Qing Lin[†,‡]

[†]Department of Physics, The Chinese University of Hong Kong, Shatin, Hong Kong SAR

[‡]Beijing Computational Science Research Center, Beijing 100084, China

Supporting Information

ABSTRACT: We show that the fluorescence emission from individual hybrid nanostructures composed of Au nanorod cores and oxazine 725-embedded mesostructured silica shells is strongly polarized, with the degree of polarization being equal to that of the light scattered by the nanorod and varying from 0 to 1 as the longitudinal plasmon resonance wavelength is increased. Our analyses indicate that the interactions of the plasmon resonance of the nanorod with the excitation and emission processes of the fluorophores are temporally separated under unsaturated excitation conditions. The emission polarization is found through electrodynamic calculations to arise from the plasmon-coupled emission instead of the plasmon-enhanced excitation polarization. The emission carries the direction and polarization properties that are essentially determined by the dipolar plasmon of the nanorod antenna. Our results therefore provide direct and concrete evidence for the plasmophore that has been proposed recently for plasmon-enhanced fluorescence.

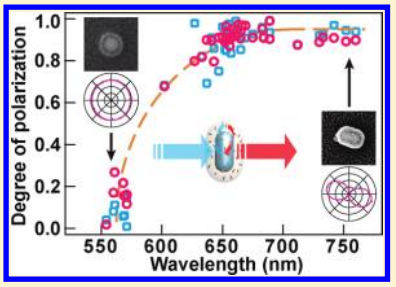

KEYWORDS: Emission polarization, energy transfer, fluorophores, gold nanorods, plasmon resonance, plasmophores

Noble metal nanostructures exhibit rich plasmonic properties. When resonantly excited, the plasmon resonance can efficiently confine the optical fields in nanoscale regions near the metal surface and enhance the local density of photonic states.[1−6] This property bridges the mismatch between the typical optical wavelengths and much smaller nanoscale optical species and paves the way to finely tailoring the interactions between light and quantum emitters such as single atoms and molecules.

Depending on the excitation and emission wavelengths of a fluorophore relative to the plasmon resonance wavelength, either or both of its excitation and emission processes can interact with the plasmon resonance. For the propagating plasmon resonances that are associated with metal−dielectric interfaces, due to the requirement of momentum matching, light can be coupled in and out of the propagating plasmon resonance only at specific angles relative to the normal of the interface. This forms the basis of the plasmon-coupled directional emission, where the emission energy is coupled from the excited state of an adjacent fluorophore to the propagating plasmon resonance through near-field interactions and then radiate to the far field at a specific direction.[7,8] Because the emitted photons carry the features of both the fluorophore and the plasmon resonance, it is difficult to tell which species is emitting. In this regard, Lakowicz et al. refer to the coupled emission system as a plasmophore,[9] which has the properties of both the fluorophore and the metal. We note that the concept of a plasmophore is different from that of a plexciton.[10] The former refers to the interactions between plasmons and fluorescence emission processes in metal−fluorophore hybrid systems, while the latter refers to the formation of hybridized states between plasmons and the excitons of dye aggregates adsorbed on metals.

The localized plasmon resonances of metal nanocrystals can also squeeze light into nanoscale regions and therefore provide a platform for the control of light−matter interactions at the nanoscale. Compared to metal−dielectric interfaces, metal nanocrystals are much more flexible in terms of their sizes, shapes, and therefore their assembly with other active components. Moreover, the absorption, scattering, and wavelength of the localized plasmon resonance can be synthetically tailored over a wide spectral range. To date, studies on the interactions of fluorophores with the localized plasmon resonances have predominantly focused on the fluorescence intensity enhancement as a function of the shape of metal nanocrystals, the plasmon resonance wavelength, and the spacing between fluorophores and metal nanocrystals.[11−29] Only in a few recent experiments have the emission properties other than the intensity been investigated. Noginov et al. demonstrated that organic fluorophores positioned around a Au nanosphere can overcome the loss of the localized plasmon resonance of the Au nanosphere by gain and realize a spaser (surface plasmon amplification by stimulated emission of radiation),[30] which is probably the smallest laser reported to date. van Hulst et al. showed that the emission polarization and direction of single fluorophores and quantum dots can be controlled by an aluminum nanoantenna fabricated at the end of an optical fiber probe[31] and Yagi−Uda antennas composed of lithographically fabricated Au nanorods.[32]

Received: February 15, 2011
Revised: April 23, 2011
Published: May 13, 2011

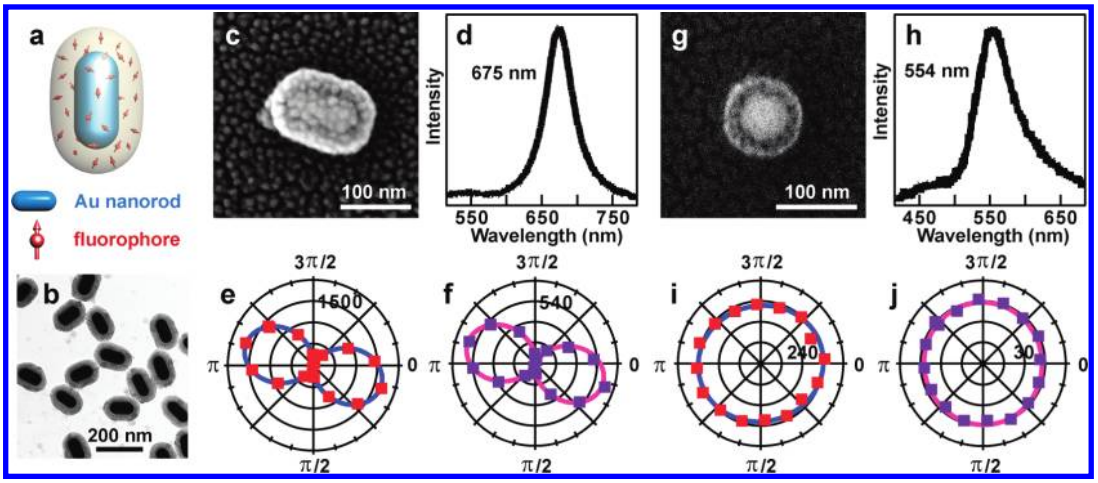

Figure 1. Emission and scattering polarization of the Au nanorod−fluorophore hybrid nanostructures: (a) schematic showing a single hybrid nanostructure; (b) TEM image of a representative nanostructure sample; (c) SEM image of a nanostructure with a nanorod core; (d−f) scattering spectrum, the polar plots of the scattering and fluorescence intensities, respectively, for the nanostructure shown in (c); (g) SEM image of a nanostructure with a nanosphere core; (h−j) scattering spectrum, the polar plots of the scattering and fluorescence intensities, respectively, for the nanostructure shown in (g). The solid curves in the polar plots are cosine squared fits.

The emission direction was found to be determined by the antenna plasmon mode irrespective of the transition dipole orientation of the quantum emitters. Although the results from these previous experiments suggest the occurrence of the energy transfer from the excited fluorophores to the localized plasmon resonances of the metals, direct evidence for the plasmophore, the emission of which possesses the properties of both the fluorophore and the metal, has remained elusive.

Here we present direct and solid evidence for the plasmophore by examining the polarization state of the emission from Au nanorod−fluorophore hybrid nanostructures at the single-particle level. The degree of polarization is measured to be equal to that of the light scattered by the nanorod, and it varies as a function of the longitudinal surface plasmon resonance (LSPR) wavelength of the nanorod. The polarized emission from the hybrid nanostructures is analyzed on the basis of the Förster resonance energy transfer from the fluorophore to the nanorod, and the spatial emission patterns are found to evolve from the molecular dipole pattern to the plasmonic dipole one as the distance between the fluorophore and the nanorod gets smaller.

We took advantage of the highly pronounced longitudinal dipolar plasmon mode of Au nanorods in our study. The LSPRs of Au nanorods are linearly polarized. Its wavelength can be finely tailored by synthetically controlling the nanorod aspect ratio. These characteristics enable us to study the emission polarization properties of the coupled system between Au nanorod antennas and fluorophores and compare them with those of the scattered light associated with the LSPR. Two Au nanorod samples and one Au nanosphere sample were prepared (see Supporting Information for the preparation details). One nanorod sample has an ensemble LSPR wavelength of 734 nm. Its diameter, length, and aspect ratio are 44 ± 3 nm, 111 ± 7 nm, and 2.5 ± 0.2, respectively (Figure S1, Supporting Information). The other nanorod sample has an ensemble LSPR wavelength of 657 nm. Its diameter, length, and aspect ratio are 48 ± 3 nm, 102 ± 5 nm, and 2.1 ± 0.2, respectively. The nanosphere sample has an ensemble plasmon resonance wavelength of 539 nm and a diameter of 42 ± 3 nm. For simplification, the nanospheres are treated as nanorods with an aspect ratio of 1. Due to the size distribution, the individual nanorods from each sample exhibit slightly different LSPR wavelengths.

The Au nanorod−fluorophore hybrid nanostructures (Figure 1a) were prepared via the formation of a mesostructured silica shell on the nanorod (see Supporting Information for the preparation details), as described previously.[25] Figure 1b shows a representative transmission electron microscopy (TEM) image of the nanorod core−silica shell nanostructures. The silica shell is uniform in thickness, with an average value of 24 ± 1 nm. After the silica coating, the LSPRs of the nanorod samples are red shifted by 10−30 nm, owing to the increase in the refractive index of the surrounding medium.[33] An organic fluorophore, oxazine 725 perchlorate, was chosen, because its emission wavelength is close to the LSPR wavelengths of the Au nanorod samples. The major absorption and emission peak wavelengths of oxazine 725 in ethanol are 645 and 662 nm, respectively. When the fluorophore molecules are embedded in the mesostructured silica, their absorption and emission peaks are red-shifted by 15 and 20 nm, respectively (Figure S2, Supporting Information). In addition, the number of the fluorophore molecules per nanostructure is estimated to be 5400 for the nanorod sample with a LSPR wavelength of 657 nm. The hybrid nanostructures were deposited on glass slides at a surface number density of ~4200 mm^{-2}. They are well-separated from each other on the glass slides.

The scattering and fluorescence properties of the hybrid nanostructures were studied on a home-built microscope (Figure S3, Supporting Information) that is capable of both imaging and spectroscopic measurements on the single-particle level.[25] A 100 W white-light lamp was utilized as the excitation source for dark-field scattering, and a 5 mW HeNe laser at 633 nm was used for fluorescence. The laser light was changed from a linear to a circular polarization state with a quarter-wave plate. A broad-band polarization analyzer was placed in front of the detector to examine the polarization-dependent intensities of both the scattering and fluorescence. The scattering and fluorescence images of the individual nanostructures were recorded consecutively as the analyzer was rotated at 22.5° per step (see Supporting Information for the scattering and fluorescence

dx.doi.org/10.1021/nl200535y |*Nano Lett.* 2011, 11, 2296–2303

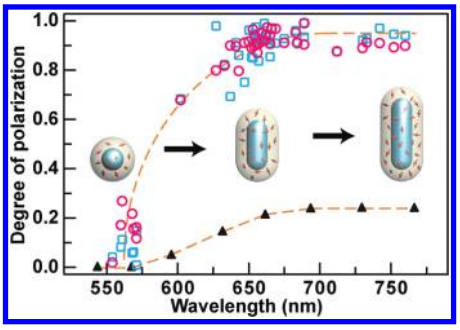

Figure 2. DOPs of the scattering (blue squares) and fluorescence emission (red circles) from the hybrid nanostructure vs the LSPR wavelength. The black solid triangles are the calculated DOPs of the plasmon-enhanced excitation electric field intensity. The dashed curves are guides for the eyes.

intensity measurement details). Each bright spot on the images was fitted with a two-dimensional Gaussian peak. The peak value was taken as the intensity. After the optical measurements, the nanostructures were sputter-coated with gold for scanning electron microscopy (SEM) imaging. The same nanostructures that were measured optically were located under the SEM imaging according to their distribution patterns on the glass slides.[25,34]

Figure 1c shows the SEM image of a typical hybrid nanostructure. Its LSPR wavelength is 675 nm (Figure 1d). Figure 1e shows the polar plot of the scattering intensity of the nanostructure as a function of the polarization angle of the analyzer. The plot can be well fitted with a cosine squared function. The scattering comes essentially from the Au nanorod core. Because the LSPR of Au nanorods is inherently polarized along the nanorod length axis, the scattered light originating from the dipolar LSPR should be also linearly polarized along the nanorod length axis.[35] Our result on the scattering is consistent with the inherent polarization nature of the LSPR. The polar plot for the scattering is oriented parallel to the nanorod length axis. After the measurement of the scattering signal, the optical microscope was switched to the fluorescence mode. Figure 1f shows the polar plot of the fluorescence intensity of the same nanostructure versus the polarization angle. The polar plot clearly shows that the fluorescence emission is highly polarized along the nanorod length axis. It looks as if the fluorescence emission is from the dipolar LSPR of the nanorod instead of the fluorophore molecules around the nanorod. This polarized emission is unexpected, because the fluorophore molecules embedded in the silica shell are essentially randomly oriented and the excitation light is circularly polarized. Under our measurement condition, the emission is expected to be completely unpolarized.

In order to ascertain the relation between the polarized emission and the plasmon resonance, we also measured the scattering and fluorescence signals from the individual nanostructures containing the Au nanospheres as the cores. Figure 1g shows the SEM image of such a nanostructure. Its scattering spectrum (Figure 1h) shows a peak at 554 nm, which arises essentially from the plasmon resonance of the Au nanosphere core. Au nanospheres have only one plasmon resonance mode. Due to the spherical symmetry, this mode can be excited under any excitation polarization direction. The scattering from the nanosphere core is therefore isotropic, which is exactly what we observe from the nanostructure (Figure 1i). Moreover, the fluorescence emission from the same nanostructure is also isotropic (Figure 1j). The isotropic emission contrasts strikingly with the strongly polarized emission observed on the nanostructures containing the Au nanorods as the cores.

For a quantitative analysis of the polarization of the scattering and fluorescence emission, a parameter, which is called the degree of polarization (DOP), is defined as

$$\mathrm{DOP} = (I_{\max} - I_{\min})/(I_{\max} + I_{\min}) \quad (1)$$

where $I_{\max}$ and $I_{\min}$ are the maximum and minimum light intensities at two perpendicular polarization directions. In the case of the Au nanorod cores, $I_{\max}$ and $I_{\min}$ represent the intensities of the light polarized parallel and perpendicular to the nanorod length axis, respectively. We carried out the optical measurements on a number of the hybrid nanostructures and determined the DOPs for both the scattering and fluorescence emission. The results are plotted as a function of the LSPR wavelength in Figure 2. The LSPR wavelengths vary from ~560 to ~770 nm. The LSPR wavelengths of Au nanorods have been known to show an approximately linear dependence on the aspect ratio.[36] After the Au nanorods are coated with a silica shell, the LSPRs are slightly red-shifted. In our experiment, the plasmon resonance wavelengths of the nanostructures containing the Au nanospheres are centered at 560 nm, and the nanostructures containing the nanorods with aspect ratios of 2.1 and 2.5 have their LSPR wavelengths clustered around 660 and 750 nm, respectively. Figure 2 shows that the DOP of the scattered light increases as the nanorod aspect ratio gets larger. The scattering DOPs for the Au nanosphere cores are within 0−0.2. The nonzero DOPs are ascribed to the presence of slightly elongated Au nanocrystals in the nanosphere sample (Figure S1b, Supporting Information). When the LSPR wavelength is longer than 650 nm, which corresponds to an aspect ratio of ~2.0 for the Au nanorod core, the scattering DOP increases to 0.8−1. The DOPs approaching 1 suggest that the scattering arising from the dipolar LSPR is nearly linearly polarized. Moreover, the trend of the DOP versus the LSPR wavelength for the fluorescence emission completely overlaps that for the scattering within the measurement error. The emission polarization of the hybrid nanostructure is strongly dependent on the aspect ratio of the Au nanorod core. When the aspect ratio is above ~2.0, the emission is almost linearly polarized along the nanorod length axis. These results indicate that the polarization of the fluorescence emission is essentially determined by the dipolar plasmon nature of the Au nanorod core.

The localized plasmon resonances have been known to play a role in both the fluorescence excitation and emission processes.[12,15,16,18,19,24−26] To scrutinize the origin of the emission polarization, we first analyze the temporal parameters involved in the fluorescence process. Given the excitation laser power density of 0.04 $W \cdot cm^{-2}$ at 633 nm and the absorption cross section of 0.013 nm^2 for oxazine 725, the interval between two consecutive excitations of a single fluorophore molecule is estimated to be 60 ms. The extinction cross sections of the Au nanorods in our experiment are estimated to be in the range of $(1-8) \times 10^4$ nm^2 according to our previous calculations.[36] The interval between two consecutive excitations of the plasmonic nanoantenna core is therefore 10−80 ns. The 6 orders of magnitude difference in the excitation frequency comes from the 6 orders of magnitude difference in their cross sections. We also measured the fluorescence lifetimes of oxazine 725 molecules embedded in the silica shell of the hybrid nanostructures

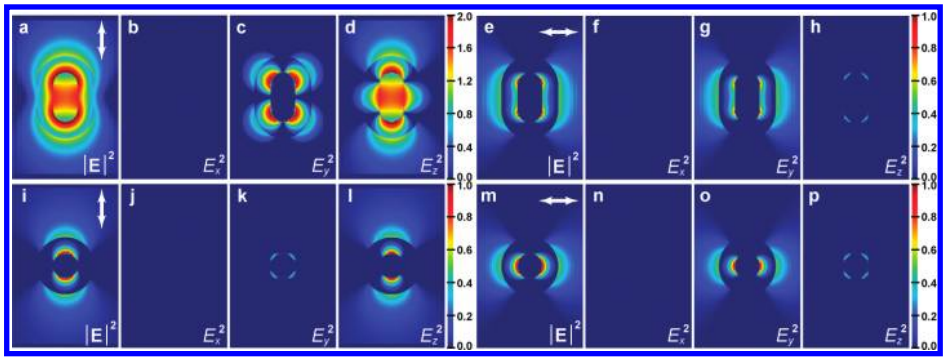

Figure 3. Contours of the electric field intensity enhancements and their components along the different axes. The *x* axis is perpendicular to the paper plane and points outward, the *y* axis points rightward, and the *z* axis points upward. The excitation light wavevector points to the negative direction of the *x* axis. The field intensity enhancements are drawn at the logarithmic scale. The contours show the enhancements on the cross section that passes through the center of the nanorod core and is parallel to the *yz* plane. The top and bottom rows are for the Au nanorod cores with aspect ratios of 2 and 1, respectively. The left four plots are for the LSPR mode, and the right four plots are for the TSPR mode.

prepared with the nanorod sample having a LSPR wavelength of 657 nm and those embedded in a mesostructured silica film that is similar to the mesostructured silica shell in terms of the mesostructure and fluorophore concentration. The lifetime measurement on the nanostructures was carried out on the ensemble level (see Supporting Information for the lifetime measurement details). The obtained lifetimes are 0.34 ± 0.01 and 1.53 ± 0.03 ns, respectively (Figure S4, Supporting Information). A comparison of the temporal parameters involved in the fluorescence process of the hybrid nanostructures with the lifetime of 10−100 fs for the localized plasmon resonances of Au nanorods[37] shows that the excitation interval of the LSPR of the Au nanorod core is much longer than both the plasmon and fluorescence lifetimes (Figure S5, Supporting Information). This implies that if a fluorophore molecule is excited by the near field of the LSPR, the molecule will decay back to the ground state before the next excitation event occurs. Furthermore, the plasmon lifetime is more than 3 orders of magnitude shorter than the fluorescence one, which means that the excited plasmon resonance will be rapidly damped while the excited fluorophore molecule will stay at the excited state for a relatively long period of time. The differences among these time parameters indicate that the excitation and emission processes are temporally separated completely. We can therefore consider the excitation and emission processes separately.

We first consider the possible effect of the plasmon-enhanced excitation on the emission polarization. During the excitation process, the transition rate of a fluorophore is proportional to the squared dot product between the transition dipole and the local electric field. Because there are a number of the fluorophore molecules in the silica shell, their transition dipoles can be assumed to be randomly oriented. We therefore just need to consider the average electric field intensity enhancements with the polarization direction oriented parallel and perpendicular to the nanorod length axis within the entire silica shell region. Suppose a hybrid nanostructure lies on the *yz* plane, with the length axis of the Au nanorod core oriented along the *z* axis. The circularly polarized excitation laser light can be decomposed as a combination of two linearly polarized light sources that are parallel to the *z* and *y* axes with an equal intensity. The two light sources therefore excite the LSPR and transverse surface plasmon resonance (TSPR) modes of the nanorod, respectively. We performed finite-difference time-domain (FDTD) calculations to obtain the electric field intensity enhancements under the excitation of the two plasmon modes (see Supporting Information for the calculation details). Cylindrical Au nanorod cores capped with a half sphere at each end were considered. The diameter of the nanorod was set at 30 nm, and the lengths were varied from 30 to 100 at 10 nm per step, corresponding to aspect ratios from 1 to 3.33, respectively. The thickness of the silica shell was set at 20 nm. The calculated LSPR wavelengths, from 544 to 767 nm (Figure S6, Supporting Information), are in the same range as those of the hybrid nanostructures prepared in our experiment. The use of the Au nanorod cores and the silica shell with sizes smaller than those of the experimental ones was to reduce the memory usage and computation time. It does not affect the result on the DOPs of the plasmon-enhanced electric field intensities. The excitation wavelength was set at 633 nm for both the LSPR and TSPR modes.

Figure 3 shows the calculated field intensity enhancement contours for the nanostructures with the Au nanorod cores having aspect ratios of 2 and 1 in the top and bottom rows, respectively. The enhancement contours for all of the differently sized nanostructures are provided in Figure S7 of the Supporting Information. Because the electric field at each point is a vector, we can decompose the local field intensity enhancement into the components along the three axes, with all of the components being relative to the excitation far field along the *y* or *z* axis. We can see that even though the excitation field is along the *z* axis for the LSPR, there exist intensity enhancements along both the *z* and *y* axes in the regions close to the nanorod ends. The two enhancement components are comparable in magnitude to each other. The same result is also observed with the TSPR. The intensity enhancement components along the *x* axis in Figure 3 and Figure S7 (Supporting Information) are zero, because the shown contours are for the cross sections that are parallel to the *yz* plane and pass through the nanorod center. There are also nonzero enhancement components along the *x* axis on the cross sections that do not pass through the nanorod center. The occurrence of the nonzero enhancement components along the directions other than the excitation field direction is due to the fact that the external electric field at the surface of an electrical conductor is always perpendicular to the surface. This can also explain why the nonzero enhancement components along the directions other than the excitation field direction are present

dx.doi.org/10.1021/nl200535y |*Nano Lett.* 2011, 11, 2296–2303

predominantly in the nanorod end regions, where the nanorod surface curvature changes abruptly.

After the field intensity enhancement components are obtained, the DOP_{ex} on the basis of the plasmon-enhanced excitation field can be determined according to

$$DOP_{ex} = \frac{(\langle E_{z,L}^2\rangle + \langle E_{z,T}^2\rangle) - (\langle E_{y,L}^2\rangle + \langle E_{y,T}^2\rangle)}{(\langle E_{z,L}^2\rangle + \langle E_{z,T}^2\rangle) + (\langle E_{y,L}^2\rangle + \langle E_{y,T}^2\rangle)} \quad (2)$$

where the averaging denoted by $\langle\rangle$ is performed over the entire silica shell and the subscripts L and T represent the LSPR and TSPR modes, respectively. In eq 2, E_y and E_z stand for the field enhancements instead of the absolute electric field values. The excitation far field is canceled. E_x is not included in eq 2, because the emitted light resulting from the excitation of the fluorophore molecules by the E_x component makes no contribution to the measured DOP values. The calculated DOP_{ex} is plotted in Figure 2 as black solid triangles. The plasmon-enhanced excitation indeed causes a certain degree of polarization for the fluorescence emission. However, the DOP_{ex} saturates at ~0.2 when the LSPR wavelength is above 650 nm. This result indicates that the nearly linearly polarized light emitted from the hybrid nanostructures cannot be accounted for by the plasmon-enhanced excitation process.

The fluorescence emission from the hybrid nanostructures exhibits the same polarization behavior as the scattered light arising from the dipolar LSPR mode. The emission seems to originate from the dipolar plasmonic nanoantenna. We therefore reason that the fluorophore near the Au nanorod core can transfer energy to the nanorod once it gets excited. The energy transfer is believed to be through the dipole−dipole near-field interaction. In the energy transfer process, the fluorophore acts as a dipolar donor, and the plasmonic Au nanorod core functions as a dipolar acceptor. This type of energy transfer has been well-known as Förster resonance energy transfer. The formulas derived on the basis of Förster resonance energy transfer can then be utilized to estimate the energy transfer rate and efficiency.

The Förster energy transfer rate $\gamma_{D\to A}$ from a dipolar donor to acceptor can be expressed as

$$\frac{\gamma_{D\to A}}{\gamma_0} = \frac{9c^4\kappa^2}{8\pi R^6}\int_0^\infty \frac{f_D(\omega)\sigma_A(\omega)}{n^4(\omega)\omega^4}\,d\omega \quad (3)$$

where γ_0 is the spontaneous decay rate of the donor to the free space in the absence of the acceptor, c is the velocity of light in vacuum, κ is the configuration function determined by the relative positions and orientations between the donor and acceptor dipoles, R is the center-to-center distance between the donor and acceptor dipoles, $n(\omega)$ is the refractive index of the medium as a function of the angular frequency ω, $f_D(\omega)$ is the normalized emission spectrum of the donor, and $\sigma_A(\omega)$ is the absorption spectrum of the acceptor. In our case, $\sigma_A(\omega)$ is the extinction spectrum of the hybrid nanostructure. Equation 3 shows that once the spectral shapes, positions, and orientations of the donor and acceptor dipoles are given, the energy transfer rate is independent of the emission intensity of the donor but dependent linearly on the absorption/extinction cross section of the acceptor. The Förster radius is often used to indicate the ease of the energy transfer from the donor to acceptor. It can be determined according to

$$R_0^6 = \frac{9c^4\kappa^2}{8\pi}\int_0^\infty \frac{f_D(\omega)\sigma_A(\omega)}{n^4(\omega)\omega^4}\,d\omega \quad (4)$$

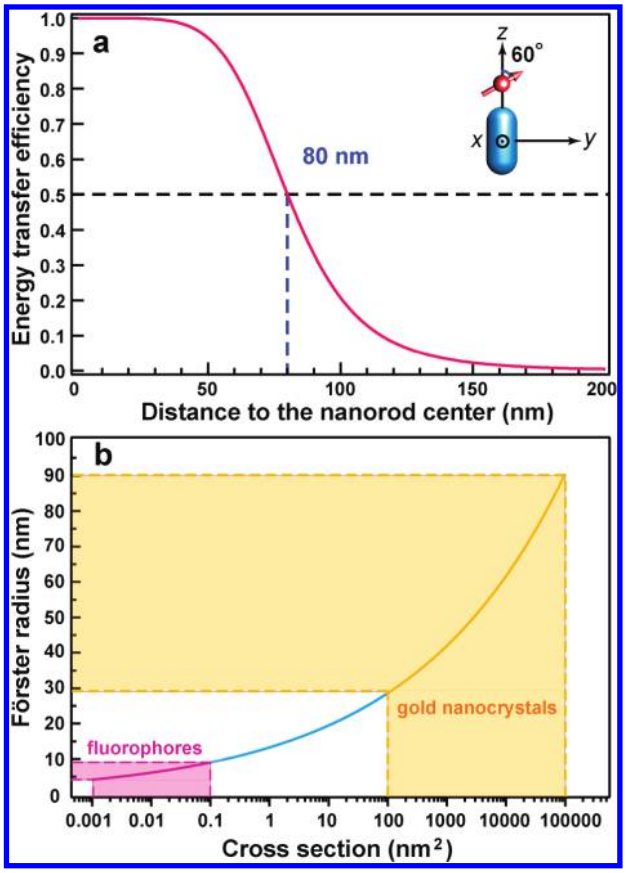

Figure 4. (a) Förster energy transfer efficiency from an oxazine 725 molecule to a Au nanorod as a function of the distance between the fluorophore and the nanorod center. The transition dipole of the fluorophore is located in the *yz* plane on the *z* axis, as shown in the inset at the top right corner. (b) Comparison of the Förster radii obtained when Au nanocrystals and organic fluorophores are used as the acceptor. The curve shows the dependence of the Förster radius on the cross section of the acceptor. The pink and orange regions indicate the typical cross sections and Förster radii for organic fluorophores and metal nanocrystals, respectively.

For the donor located at the Förster radius apart from the acceptor, the energy transfer rate $\gamma_{D\to A}$ is equal to the decay rate γ_0. The energy transfer efficiency η is defined as the fraction of the decay rate arising from the energy transfer within the total decay rate of the donor and given by

$$\eta = \frac{\gamma_{D\to A}}{\gamma_0 + \gamma_{D\to A}} = \frac{1}{1 + (R/R_0)^6} \quad (5)$$

The emission spectrum of oxazine 725 dissolved in ethanol (Figure S2, Supporting Information) and the extinction spectrum of the Au nanorod core−silica shell nanostructure containing a 30 nm thick and 70 nm long nanorod core (Figure S8, Supporting Information) were utilized for the estimation of the Förster energy transfer efficiency and radius (see Supporting Information for the estimation details). The absorption and emission spectra of oxazine 725 dissolved in water at low concentrations are nearly the same as those in ethanol. The choice of the core−shell nanostructure with the nanorod core having an aspect ratio of 2.33 is because its LSPR wavelength is nearly equal to the main emission peak wavelength of oxazine 725. Figure 4a shows the energy transfer efficiency as a function

dx.doi.org/10.1021/nl200535y |*Nano Lett.* 2011, 11, 2296–2303

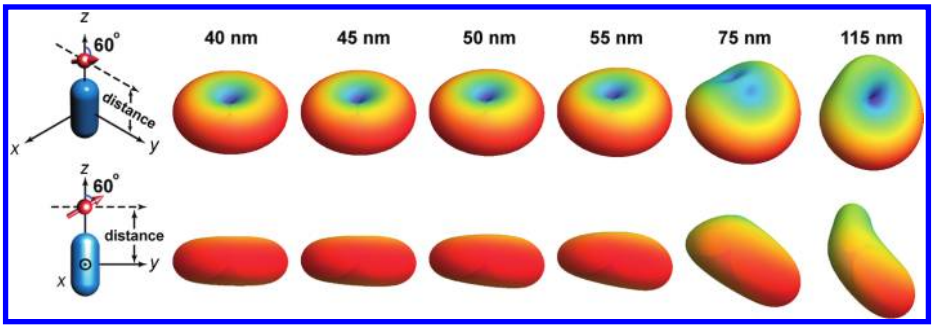

Figure 5. Far-field emission patterns of a dipole source placed at varying distances away from the nanorod. The dipole is located at one end of the nanorod in the *yz* plane. The patterns in the top row are in a tilted view, while the corresponding ones in the bottom row are viewed along the *x* axis. The distances between the dipole and the center of the nanorod are indicated at the top.

of the distance between the fluorophore and the center of the nanorod . In this example, the molecular dipole is located at one end of the nanorod in the *yz* plane and forms an angle of 60° with the *z* axis. The Förster radius is calculated to be 80 nm. When the molecular dipole is positioned at the side of the nanorod in the *yz* plane and forms an angle of 60° with the *z* axis, the Förster radius is calculated to be 63 nm (Figure S9, Supporting Information). In both cases, when the dipole is located within a distance of 20 nm away from the nanorod surface, the energy transfer efficiency increases above 0.9 and approaches to 1.0. In our experiment, the silica shells of the hybrid nanostructures have an average thickness of 24 nm. The obtained results on the energy transfer efficiency suggest that most of the fluorophore molecules in the silica shell, except those with their dipoles oriented perpendicular to the plasmonic dipole of the nanorod, transfer their excited energy to the nanorod antenna at an efficiency of nearly 100%.

We also calculated the Förster radii for the energy transfer from oxazine 725 to either organic fluorophores or Au nanocrystals (Figure 4b). The absorption peak wavelengths of organic fluorophores and the plasmon resonance wavelengths of Au nanocrystals are chosen to be nearly the same as the emission peak wavelength of oxazine 725. The Förster radii with typically sized Au nanocrystals range from 30 to 90 nm, while those with organic fluorophores as the acceptors are in the range of 5−10 nm. The former are generally 1 order of magnitude larger than the latter. This is because the extinction cross sections of Au nanocrystals are 3−8 orders of magnitude larger than the absorption cross sections of organic fluorophores. The use of Au nanocrystals as acceptors therefore provides a potential means for controlling the Förster radius and thus the energy transfer efficiency by synthetically tailoring the nanocrystal shape and size while keeping the plasmon resonance wavelength unchanged.[36,38,39] We also note that the volume of the Au nanorod core in our estimation of the Förster radius is ∼3.5-fold smaller than that in our experiment. If we take the extinction cross sections of Au nanocrystals to be proportional to the nanocrystal volume, the Förster radius for the Au nanocrystals used in our experiment will be ∼1.2-fold larger than that in the calculation. In addition, the Au nanocrystals with LSPR energies being degenerate with the emission peak energy of oxazine 725 are considered in our estimation. Small displacements of the plasmon resonance peak away from the emission peak will not severely affect our result on the energy transfer radius and efficiency, because the plasmon resonance peak widths of the Au nanorods are ∼1.2-fold larger than the emission peak width of oxazine 725, and the plasmon resonance peak widths of the Au nanospheres are 2−5-fold larger than those of the Au nanorods.[37] There will be considerable spectral overlap between the emission peak of the fluorophore and the plasmon resonance peak of the Au nanocrystals despite the small spectral displacements.

We further performed FDTD calculations to simulate the emission patterns of a fluorophore placed at varying distances away from a Au nanorod. In our simulation, a 30 nm thick and 70 nm long nanorod is positioned at the origin, with its length axis along the *z* axis. The fluorophore is represented by a Hertzian dipole, which is located in the *yz* plane and forms an angle of 60° with the *z* axis. The emission wavelength of the dipole is 670 nm, which is nearly equal to the LSPR wavelength of the Au nanorod. The entire system is immersed in water. The nanorod is uncoated in order to eliminate the possible effects of the nonuniform surrounding medium on the far-field emission pattern. The LSPR is excited by the dipolar source. The power flow is detected by a frequency-domain power monitor placed at a distance of 800 nm away from the nanorod and projected to the far field to generate the emission pattern. Figure 5 shows the emission patterns when the dipole is placed at one end of the nanorod. When the gap distance between the dipole and the nanorod surface is smaller than ∼20 nm, the far-field emission pattern is doughnut-shaped and symmetrical about the *z* axis. It carries the property of the plasmonic dipole. As the gap distance is increased, the far-field emission pattern evolves gradually and is finally determined mainly by the molecular dipole. This variation trend is consistent with that of the Förster energy transfer efficiency, which becomes smaller as the gap distance is increased.

Figure S10 (Supporting Information) shows the emission patterns when the dipole is placed at one side of the nanorod. A similar distance-dependent evolution behavior of the emission pattern is observed. One difference is that the gap distance at which the emission pattern starts to lose the plasmonic dipole nature is smaller than that when the dipole is positioned at the end of the nanorod. This result is again consistent with that obtained in the estimation of the Förster radius. The Förster radius calculated when the molecular dipole donor is positioned at the side of the nanorod is smaller than that when the molecular dipole is located at the end.

The fluorophore molecules in our hybrid nanostructures are all embedded within the silica shell. The maximum distance from the fluorophore molecules to the Au nanorod surface is determined by the shell thickness, which is 24 nm in our experiment. On the basis of the results and discussions above, most of the fluorophore molecules transfer their energy to the plasmonic Au nanorod antenna during their spontaneous decay. The Au nanorod

dx.doi.org/10.1021/nl200535y |*Nano Lett.* 2011, 11, 2296–2303

core accepts the energy and radiates, with the polarization and direction properties of the emitted light determined by the plasmonic dipole. This is the reason the linearly polarized fluorescence emission is observed from the individual hybrid nanostructures. To date, in most of the studies on the interactions between plasmonic nanoantennas and fluorophores, except those employing pulsed lasers, the excitation is unsaturated. Under unsaturated excitation conditions, the interactions between a plasmonic nanoantenna and a fluorophore, that is, a plasmophore, are composed of two temporally separated processes (Figure S11, Supporting Information). The first is the excitation process, where the excitation rate of the fluorophore is increased due to the enhanced electric field near the nanoantenna. The second one is the coupled emission from the nanoantenna−fluorophore hybrid system through the Förster energy transfer from the fluorophore to nanoantenna. The energy transfer process can not only enhance the radiative and nonradiative decay rates and thus alter the quantum yield of the fluorophor,[12,15,16,24,27,29] but also lead to the emission of light that carries the polarization and direction properties of the plasmonic nanoantenna dipole.

In conclusion, we have shown that the fluorescence emission from the individual Au nanorod−fluorophore hybrid nanostructures is strongly polarized. The emission is found to be polarized along the length axis of the nanorod, with the degree of polarization being strongly dependent on the aspect ratio of the nanorod. The interactions between the plasmonic nanorod antenna and the fluorophore molecules can be separated temporally into plasmon-enhanced excitation and coupled emission processes under unsaturated excitation conditions. Our electrodynamic calculations show that the emission polarization cannot be accounted for by plasmon-enhanced excitation. The emission essentially comes from the plasmonic nanorod antenna, which accepts energy from the excited fluorophore molecules. The Förster radius for the energy transfer from the molecular fluorophore to the plasmonic nanoantenna is estimated to be 1 order of magnitude larger than that between two fluorophore molecules. The far-field emission patterns of the hybrid nanostructures further reveal that the emitted light carries the feature of the plasmonic nanoantenna. The emission patterns evolve from the plasmonic dipole nature to the molecular dipole nature as the gap distance between the fluorophore molecule and the nanorod surface is gradually increased. Our results provide strong evidence for the use of the plasmophore to describe the light emission from the hybrid nanostructures composed of noble metal nanocrystals and fluorophores. They also point out a potential way of using plasmonic nanoantennas to control the emission properties, such as polarization and direction, of quantum systems.

■ ASSOCIATED CONTENT

Supporting Information. The growth of the nanorods and nanospheres, preparation of the nanostructures, measurements of the fluorescence intensity and lifetime, FDTD calculations, estimation of the Förster radius and energy transfer efficiency, extinction spectra and TEM images of the Au nanocrystals, absorption and emission spectra of oxazine 725, schematic of the fluorescence measurement system, fluorescence decay curves, typical values of the temporal parameters involved in the fluorescence process, calculated scattering, extinction spectra and field intensity enhancement contours, energy transfer efficiencies, far-field emission patterns, and schematic of a plasmophore. This material is available free of charge via the Internet at http://pubs.acs.org.

■ AUTHOR INFORMATION

Corresponding Author
*E-mail: jfwang@phy.cuhk.edu.hk.

■ ACKNOWLEDGMENT

This work was supported by CUHK block grant (project code: 3110061), the MOST of China (Grant No.: 2011CB922200), and RGC Direct Allocation (Project Code: 2060393).

■ REFERENCES

(1) Martin, O. J. F.; Girard, C.; Dereux, A. *Phys. Rev. Lett.* **1995**, *74*, 526–529.
(2) Mühlschlegel, P.; Eisler, H.-J.; Martin, O. J. F.; Hecht, B.; Pohl, D. W. *Science* **2005**, *308*, 1607–1609.
(3) García de Abajo, F. J.; Kociak, M. *Phys. Rev. Lett.* **2008**, *100*, 10684.
(4) Schnell, M.; García-Etxarri, A.; Huber, A. J.; Crozier, K.; Aizpurua, J.; Hillenbrand, R. *Nat. Photonics* **2009**, *3*, 287–291.
(5) Hohenester, U.; Ditlbacher, H.; Krenn, J. R. *Phys. Rev. Lett.* **2009**, *103*, 106801.
(6) Schuller, J. A.; Barnard, E. S.; Cai, W. S.; Jun, Y. C.; White, J. S.; Brongersma, M. L. *Nat. Mater.* **2010**, *9*, 193–204.
(7) Lakowicz, J. R. *Anal. Biochem.* **2004**, *324*, 153–169.
(8) Gryczynski, I.; Malicka, J.; Gryczynski, Z.; Lakowicz, J. R. *Anal. Biochem.* **2004**, *324*, 170–182.
(9) Lakowicz, J. R.; Ray, K.; Chowdhury, M.; Szmacinski, H.; Fu, Y.; Zhang, J.; Nowaczyk, K. *Analyst* **2008**, *133*, 1308–1346.
(10) Fofang, N. T.; Park, T.-H.; Neumann, O.; Mirin, N. A.; Nordlander, P.; Halas, N. J. *Nano Lett.* **2008**, *8*, 3481–3487.
(11) Song, J.-H.; Atay, T.; Shi, S. F.; Urabe, H.; Nurmikko, A. V. *Nano Lett.* **2005**, *5*, 1557–1561.
(12) Liu, N. G.; Prall, B. S.; Klimov, V. I. *J. Am. Chem. Soc.* **2006**, *128*, 15362–15363.
(13) Mertens, H.; Biteen, J. S.; Atwater, H. A.; Polman, A. *Nano Lett.* **2006**, *6*, 2622–2625.
(14) Pompa, P. P.; Martiradonna, L.; Dela Torre, A.; Della Sala, F.; Manna, L.; de Vittorio, M.; Calabi, F.; Cingolani, R.; Rinaldi, R. *Nat. Nanotechnol.* **2006**, *1*, 126–130.
(15) Anger, P.; Bharadwaj, P.; Novotny, L. *Phys. Rev. Lett.* **2006**, *96*, 113002.
(16) Kühn, S.; Håkanson, U.; Rogobete, L.; Sandoghdar, V. *Phys. Rev. Lett.* **2006**, *97*, 017402.
(17) Aslan, K.; Wu, M.; Lakowicz, J. R.; Geddes, C. D. *J. Am. Chem. Soc.* **2007**, *129*, 1524–1525.
(18) Tam, F.; Goodrich, G. P.; Johnson, B. R.; Halas, N. J. *Nano Lett.* **2007**, *7*, 496–501.
(19) Chen, Y.; Munechika, K.; Ginger, D. S. *Nano Lett.* **2007**, *7*, 690–696.
(20) Zhang, J.; Fu, Y.; Chowdhury, M. H.; Lakowicz, J. R. *Nano Lett.* **2007**, *7*, 2101–2107.
(21) Guo, S.-H.; Tsai, S.-J.; Kan, H.-C.; Tsai, D.-H.; Zachariah, M. R.; Phaneuf, R. J. *Adv. Mater.* **2008**, *20*, 1424–1428.
(22) Bek, A.; Jansen, R.; Ringler, M.; Mayilo, S.; Klar, T. A.; Feldmann, J. *Nano Lett.* **2008**, *8*, 485–490.
(23) Mackowski, S.; Wörmke, S.; Maier, A. J.; Brotosudarmo, T. H. P.; Harutyunyan, H.; Hartschuh, A.; Govorov, A. O.; Scheer, H.; Brauchle, C. *Nano Lett.* **2008**, *8*, 558–564.
(24) Bardhan, R.; Grady, N. K.; Cole, J. R.; Joshi, A.; Halas, N. J. *ACS Nano* **2009**, *3*, 744–752.

(25) Ming, T.; Zhao, L.; Yang, Z.; Chen, H. J.; Sun, L. D.; Wang, J. F.; Yan, C. H. *Nano Lett.* **2009**, *9*, 3896–3903.
(26) Kinkhabwala, A.; Yu, Z. F.; Fan, S. H.; Avlasevich, Y.; Müllen, K.; Moerner, W. E. *Nat. Photonics* **2009**, *3*, 654–657.
(27) Viste, P.; Plain, J.; Jaffiol, R.; Vial, A.; Adam, P. M.; Royer, P. *ACS Nano* **2010**, *4*, 759–764.
(28) Fu, Y.; Zhang, J.; Lakowicz, J. R. *J. Am. Chem. Soc.* **2010**, *132*, 5540–5541.
(29) Munechika, K.; Chen, Y.; Tillack, A. F.; Kulkarni, A. P.; Plante, I. J.-L.; Munro, A. M.; Ginger, D. S. *Nano Lett.* **2010**, *10*, 2598–2603.
(30) Noginov, M. A.; Zhu, G.; Belgrave, A. M.; Bakker, R.; Shalaev, V. M.; Narimanov, E. E.; Stout, S.; Herz, E.; Suteewong, T.; Wiesner, U. *Nature* **2009**, *460*, 1110–1112.
(31) Taminiau, T. H.; Stefani, F. D.; Segerink, F. B.; van Hulst, N. F. *Nat. Photonics* **2008**, *2*, 234–237.
(32) Curto, A. G.; Volpe, G.; Taminiau, T. H.; Kreuzer, M. P.; Quidant, R.; van Hulst, N. F. *Science* **2010**, *329*, 930–933.
(33) Chen, H. J.; Kou, X. S.; Yang, Z.; Ni, W. H.; Wang, J. F. *Langmuir* **2008**, *24*, 5233–5237.
(34) Chen, H. J.; Sun, Z. H.; Ni, W. H.; Woo, K. C.; Lin, H.-Q.; Sun, L. D.; Yan, C. H.; Wang, J. F. *Small* **2009**, *5*, 2111–2119.
(35) Schubert, O.; Becker, J.; Carbone, L.; Khalavka, Y.; Provalska, T.; Zins, I.; Sönnichsen, C. *Nano Lett.* **2008**, *8*, 2345–2350.
(36) Ni, W. H.; Kou, X. S.; Yang, Z.; Wang, J. F. *ACS Nano* **2008**, *2*, 677–686.
(37) Sönnichsen, C.; Franzl, T.; Wilk, T.; von Plessen, G.; Feldmann, J.; Wilson, O.; Mulvaney, P. *Phys. Rev. Lett.* **2002**, *88*, 077402.
(38) Chen, H. J.; Shao, L.; Woo, K. C.; Ming, T.; Lin, H.-Q.; Wang, J. F. *J. Phys. Chem. C* **2009**, *113*, 17691–17697.
(39) Chen, H. J.; Shao, L.; Ming, T.; Sun, Z. H.; Zhao, C. M.; Yang, B. C.; Wang, J. F. *Small* **2010**, *6*, 2272–2280.